Quantized antiferromagnetic spin waves in the molecular Heisenberg ring CsFe$_8$

J. Dreiser[*] and O. Waldmann[†]

Physikalisches Institut, Universität Freiburg, D-79104 Freiburg, Germany

C. Dobe, G. Carver, S. T. Ochsenbein, A. Sieber, and H. U. Güdel
Department of Chemistry and Biochemistry, University of Bern, 3012 Bern, Switzerland

J. van Duijn and J. Taylor
ISIS Facility, Rutherford Appleton Laboratory, Chilton, Didcot, Oxfordshire OX11 0QX, United Kingdom

A. Podlesnyak[‡]
Paul Scherrer Institute, CH-5232 Villigen, Switzerland

We report on inelastic neutron-scattering (INS) measurements on the molecular spin ring CsFe$_8$, in which eight spin-5/2 Fe(III) ions are coupled by nearest-neighbor antiferromagnetic Heisenberg interaction. We have recorded INS data on a nondeuterated powder sample up to high energies at the time-of-flight spectrometers FOCUS at PSI and MARI at ISIS, which clearly show the excitation of spin waves in the ring. Due to the small number of spin sites, the spin-wave dispersion relation is not continuous but quantized. Furthermore, the system exhibits a gap between the ground state and the first excited state. We have modeled our data using exact diagonalization of a Heisenberg-exchange Hamiltonian together with a small single-ion anisotropy term. Due to the molecule's symmetry, only two parameters J and D are needed to obtain excellent agreement with the data. The results can be well described within the framework of the rotational-band model as well as antiferromagnetic spin-wave theories.

PACS number(s): 75.50.Xx, 75.10.Jm, 78.70.Nx

I. INTRODUCTION

In recent years, large progress has been made in the understanding and control of mesoscopic magnetic systems, which is driven by the interest in fundamental research as well as potential applications in molecular devices.[1–5] Dimensionality plays a key role here: magnetic confinement in one or more dimensions leads to strong changes in the density of states, i.e., quantization effects occur,[6–12] which become more pronounced with lower dimensionality. Theoretical work on spin waves in low-dimensional antiferromagnetic (AFM) systems reaches back to the early 1950s. While low-temperature thermodynamical properties in two and three dimensions are well described by a conventional spin-wave approach, the case of one dimension (1D) is more difficult due to divergencies in the sublattice magnetization.[13,14] These divergencies are deeply rooted in the fact that, by construction, spin-wave theory (SWT) starts out from the assumption of a long-range ordered ground state, and their appearance provides a hint to the nature of the ground state, i.e., whether it is disordered (divergency) or long-range ordered (no divergency). However, despite these subtleties it has been found that also for disordered systems SWTs can produce results of high accuracy, e.g., for the ground-state energy.[13] Furthermore, the divergencies could subsequently be removed by introducing constraints on the sublattice magnetization in the so-called modified SWTs (Refs. 15–20) and finite-size SWTs.[21–23] This establishes a significant improvement but nevertheless the applicability of SWTs to disordered systems remains a topic of current research. Formerly, the main focus of the theoretical and experimental activities has been on systems of infinite

extension,[24,25] and it has only been in recent years that research on finite, or zero-dimensional (0D), systems has been intensified. In this context, the topic of quantized spin waves in mesoscopic spin clusters has been investigated.[8,26–32]

A good physical realization of such mesoscopic spin clusters are molecular nanomagnets.[33] They have been shown to be a vast experimental playground enabling the study of precisely defined clusters with chemically engineered exchange couplings and magnetic anisotropy, or topology. So far, a variety of mesoscopic and quantum phenomena such as tunneling of the magnetization and stepwise change in the magnetization have been demonstrated (for reviews see Refs. 33–37). A particularly intriguing type of spin clusters are AFM Heisenberg rings in which a number of magnetic metal ions are arranged in the shape of a ring with nearest-neighbor AFM Heisenberg couplings. The Hamiltonian describing their magnetism is given in its simplest form by

$$\hat{H} = -J\left(\sum_{i=1}^{N-1} \hat{s}_i\hat{s}_{i+1} + \hat{s}_N\hat{s}_1\right) \quad (1)$$

with $J < 0$ the magnetic coupling strength, N the number of magnetic sites, and $\hat{s}_i$ the spin operator of the ith ion with spin s. Their magnetism and spin dynamics have intensely been studied by a host of different experimental techniques;[38–43] the recent experimental work on a Cr$_8$ spin-3/2 ring has probably most clearly demonstrated the nature of the elementary excitations.[30]

On the theory side, the rotational-band model (RBM) has been established,[44–50] and there has been striking experimental evidence that this picture is a good description for a va-

riety of finite, bipartite AFM spin clusters with varying topologies[51–56] as well as some frustrated systems,[57–59] but of course also exceptions exist.

The RBM classifies the lowest-lying magnetic excitations into two bands with a parabolic energy dependence on S, the L, and E band (S is the total spin quantum number). Physically, the L band can be interpreted as rotations of the two AFM sublattices and is, so to say, a precursor of a long-range Néel-ordered ground state in the infinite lattice (it is also known as the tower of states or quasidegenerate joint states[45,46]). In contrast, the E-band states can be associated with quantized spin-wave excitations.[49,60] For both bands, the energies are proportional to $S(S+1)$ but the E band consists of several subbands which are shifted up in energy by constant offsets. For $S \geq 1$, this can be summarized as

$$E(S,k) = \frac{1}{2}\epsilon(\pi)S(S+1) + \epsilon(k) - \epsilon(\pi) \qquad (2)$$

with $k=0$ or π for the L band, where $\epsilon(k)$ may be regarded as the finite-size version of a spin-wave dispersion relation, and k would become a wave vector in an infinite system.

There are several reasons for classifying the low-lying excitations into L and E band: the spectrum of a conventional SWT exhibits zero-energy (Goldstone) modes, with wave vector $k=0,\pi$, reflecting the (assumed or factual) long-range order, which in the context of extended magnets are included in the notation of spin waves or magnons. However, in a finite system these $k=0,\pi$ modes exhibit a gap with respect to the ground-state energy, forming the L band. These excitations are hence of different physical significance than the higher-lying magnon states (E band). The different nature of the L and E band is further manifested by the fact, that only the $k=0,\pi$ modes are responsible for the diverging sublattice magnetizations in the conventional SWTs, that the L- and E-band states have different sublattice lengths, and that the scaling with N is generally different. In addition, this distinction is supported by a selection rule for the inelastic neutron-scattering (INS) intensities, which at low temperatures allows only INS transitions between L-band states or from L-band to E-band states.[49] This key characteristic has been experimentally demonstrated in great detail.[30] Owing to the obviously different physical properties in small systems, the L-band states should be distinguished from the spin waves or magnons.

In the above description, the lowest excited state of an AFM Heisenberg ring is the $S=1$ state of the L band, which to a good approximation has a gap of $\Delta_c = 4|J|/N$ to the $S=0$ ground state. Obviously, Δ_c vanishes for $N \rightarrow \infty$; it is thus a property of finite rings. In this context, Haldane's conjecture[61] should also be mentioned. It predicts that integer-spin 1D chains exhibit a gap in the energy spectrum while half-integer 1D spin chains do not. In small rings, however, there is numerical evidence that the gap is largely dominated by Δ_c without discriminating integer or half-integer spin.[49,62,63] This criterion, in fact, may be regarded as a definition of what we mean by "small" or "0D." A further consequence of the small size is obviously that the spin waves become quantized, as there can be at most as many spin-wave modes as there are spin sites in the cluster (the
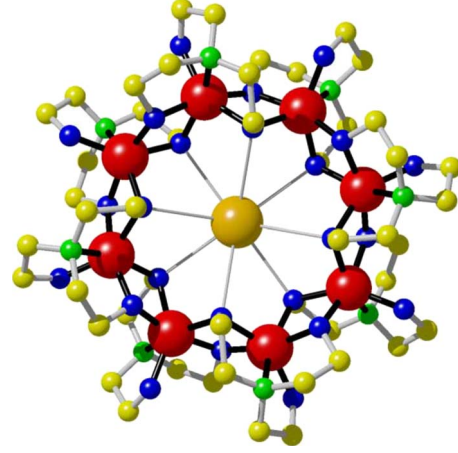

FIG. 1. (Color online) Crystal structure of $CsFe_8$ [with Fe as dark gray spheres (red online) and H atoms omitted].

number of spin waves is slightly smaller than N, for even AFM rings it is $N-2$).

In this work we investigate the molecule $[CsFe_8\{N(CH_2CH_2O)_3\}_8]Cl$ or $CsFe_8$ in short (Fig. 1). By a variety of experimental techniques, such as high-field torque magnetometry and INS, the $CsFe_8$ molecule has been demonstrated to be a good model system for an AFM Heisenberg ring.[64,65] It is characterized by eight Fe(III) ions ($s=5/2$), which form an almost planar ring with a crystallographic C_4 symmetry axis (z axis) perpendicular to the wheel plane. The $CsFe_8$ molecule was shown to be very well described by a generic spin Hamiltonian with dominant nearest-neighbor AFM Heisenberg couplings plus an uniaxial single-ion anisotropy term,

$$\hat{H} = -J\left(\sum_{i=1}^{N-1} \hat{s}_i \hat{s}_{i+1} + \hat{s}_N \hat{s}_1\right) + D\sum_{i=1}^{N} \hat{s}_{i,z}^2. \qquad (3)$$

All the previous experimental data can consistently be described, with an accuracy margin of few percents, with the values $J=-1.79$ meV and $D=-0.05$ meV. However, all these experiments were only sensitive to the L band states. Here we extend the studies to higher energies, allowing for an investigation of the E-band states. The presented INS data will experimentally confirm the expected quantized spin-wave modes, complete the picture of the excitation modes in the $CsFe_8$ molecule, and thus establish the only second example of a full experimental test of the RBM in a small spin cluster. Furthermore, we will describe the E-band excitations by different SWTs, comparing their performance to each other. This provides insight into their merits and drawbacks when applied to mesoscopic spin clusters.

The paper is organized as follows: in the experimental Sec. II the INS spectra and $S(Q,\omega)$ plots are presented. Further, in Sec. III the INS experiments are described in terms of the microscopic spin Hamiltonian (3). In Sec. IV the E-band excitations are discussed in a more general fashion, revealing their spin-wave character and testing different SWTs. Finally, Sec. V contains the summary and concludes the paper.
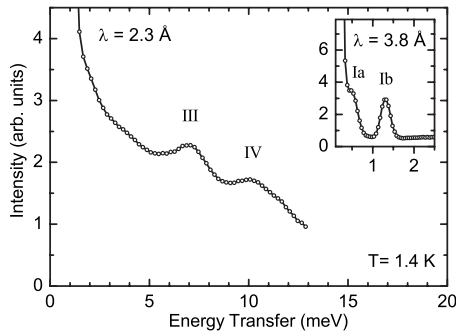
FIG. 2. INS spectra taken on FOCUS at a temperature of T =1.4 K and wavelengths λ=2.3 Å (main panel) and 3.8 Å (inset).

II. EXPERIMENTS

A powder sample of $CsFe_8$ was prepared according to literature procedures using nondeuterated starting materials.[64] INS data were recorded on the direct time-of-flight spectrometer FOCUS at the Paul Scherrer Institute (Villigen, Switzerland) using neutrons with incident wavelengths λ=2.3 and 3.8 Å, and the MARI spectrometer at the pulsed neutron source ISIS (Didcot, U.K.) using neutrons with incident energies of E_i=15 and 25 meV. The experimental resolutions at the elastic line were 1.13 and 0.28 meV for the FOCUS, and 0.39 and 0.72 meV for the MARI experiments. If not stated otherwise, the data were summed over all detector banks and the neutron-energy-loss side is shown.

Figure 2 presents the 2.3 Å FOCUS data taken at a temperature of T=1.4 K. Clearly, two cold peaks at energy transfers of approximately 7 meV (peak III) and 10 meV (peak IV) are visible. The 3.8 Å spectrum, shown in the inset of Fig. 1, reveals two additional low-energy peaks at energy transfers of about 0.5 meV (peak Ia) and 1.3 meV (peak Ib). Figure 3 shows INS spectra recorded on MARI at temperatures of 5–58 K. The peaks Ib, III, and IV can again be observed, but thanks to the larger energy range and higher resolution, additional features become visible. In particular, a further peak at about 2.3 meV (peak II) is resolved in the 15 meV data (inset of Fig. 3). An inspection of the temperature dependence of these four peaks suggests that they are cold transitions and of magnetic origin. Additional features can be
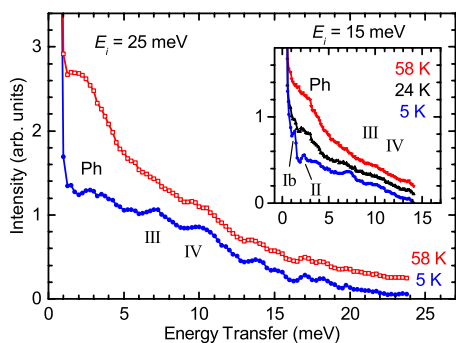

FIG. 3. (Color online) Temperature dependence of the INS spectra as recorded on MARI for incident neutron energies of 25 meV (main panel) and 15 meV (inset). Intensity was summed over all detector banks.
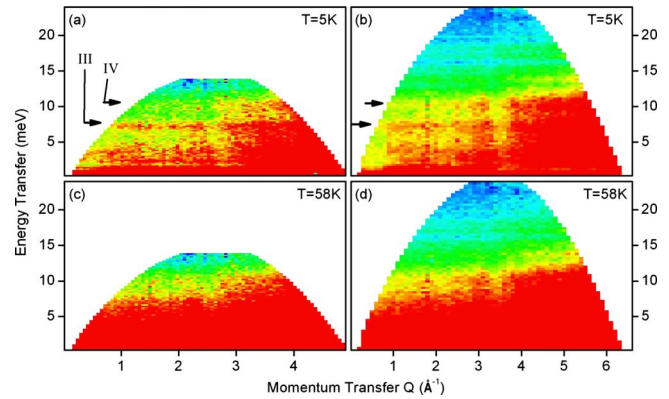

FIG. 4. (Color online) $S(Q,w)$ plots for the temperatures T =5 K (upper plots) and 58 K (lower plots) for the two incident neutron energies E_i=15 meV (left) and 25 meV (right) as measured on MARI. The intensity is color coded (blue=low, red =high intensity); the color scale is identical for each of the four plots.

observed, such as the broad feature at about 2.5 meV (feature marked by "Ph") in the high-temperature data and the many features at energy transfers above 13 meV. Their temperature dependence suggests a phononic origin.

The observed low-energy peaks Ia, Ib, and II are fully consistent with the previous investigations on this molecule, in particular, the INS experiments.[66,67] Peaks Ia and Ib correspond to the transitions from the $S=0$ ground state to the first excited $S=1$ level, which is split by magnetic anisotropy into its components $M=0$ and $M=\pm 1$ (M is the magnetic quantum number of the total spin S). Peak II corresponds to the transition from the lowest excited state to the first excited $S=2$ level. The transitions III and IV were hitherto not observed; their observation and identification as spin waves form the main body of this work. In the following, we will analyze the data more carefully in order to demonstrate the magnetic nature of the peaks I to IV, and the lattice origin of the other features in the spectra. In doing so, we will focus on the two peaks III and IV (as the magnetic peaks at lower energies are already well understood).

First, we analyze the full $S(Q,\omega)$ dependence as presented in Fig. 4 for the temperatures 5 and 58 K and settings E_i=15 and 25 meV. The Q dependence of the scattering intensity allows a clear differentiation: the magnetic scattering is determined by the magnetic form factors of the involved metal ions and interference factors reflecting their spatial arrangement,[68] it is hence most significant at lower Q values. In contrast, the phonon-scattering intensity increases with Q as Q^2. In the low-temperature data, peaks III and IV (marked by black arrows) are visible in the whole Q range, in particular, at small Q values, which strongly supports a magnetic origin of these peaks. In the high Q regime the phonon-induced scattering clearly dominates. The phonon scattering also increases strongly with temperature, as demonstrated by the 58 K data, where scattering is dominated by phonons at all momentum transfers.

Figure 5 shows cuts along the energy axis of the 5 K spectra for three different regimes of momentum transfer (lowest, black curve; middle, red curve; upper, green curve).
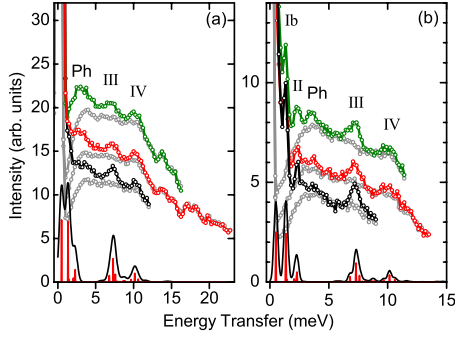
FIG. 5. (Color online) Q slices for (a) the $E_i = 25$ meV and (b) the $E_i = 15$ meV data at $T = 5$ K. In panel (a), the lowest (black), middle (red), and upper (green) curves correspond to $Q \in [1.0, 2.5[$, $[2.5, 4.0[$, and $[4.0, 5.5[$ Å^{-1}, and in panel (b) to $Q \in [1.0, 2.0[$, $[2.0, 3.0[$, and $[3.0, 4.0]$ Å^{-1}. The curves have been offset in order to improve visibility. The gray curves represent the Bose-factor corrected 58 K data as discussed in the text. The solid lines at the bottom are calculated INS spectra obtained with the best-fit parameters. The spikes (red) mark the exact position and relative scattering strengths of the individual INS transitions, the solid (black) curve was obtained by convolution with a Gaussian accounting for the experimental resolution.

It reveals that the intensity of the peaks Ib, II, III, and IV roughly stays constant with Q. It might be surprising that these peaks exhibit significant intensity even at Q values as large as approximately 4 Å, where the magnetic form factors have already dropped considerably; we attribute this to a strong incoherent scattering in our nondeuterated sample smearing out the Q dependence. These plots further demonstrate that the feature at approximately 2.5 meV (compare with Fig. 2) must indeed be a phonon.

In Fig. 5, the gray curves were obtained by scaling the $T = 58$ K data by the Bose factor $[1 - \exp(-\hbar\omega/k_B T)]^{-1}$, which governs the temperature dependence of phonon scattering.[69] Considering that at high temperatures the magnetic scattering intensity is strongly reduced as it spreads out over essentially all energies, this curve should provide an estimate of the phonon background. A comparison with the 5 K data nicely confirms the magnetic nature of peaks III and IV, and also proves that the scattering at higher energies above 12 meV is purely phononic. The data after correction by the Bose factor is shown in Fig. 6(a) as a $S(Q, \omega)$ plot for
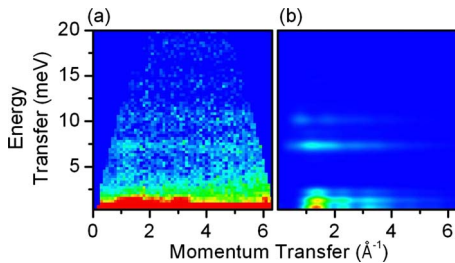

FIG. 6. (Color online) (a) $S(Q, \omega)$ plot of the $E_i = 25$ meV MARI data at $T = 5$ K after subtraction of the phonon background as described in the text. (b) $S(Q, \omega)$ plot ($T = 5$ K) as calculated from the spin Hamiltonian (3) with the parameters $J = -1.79$ meV and $D = -0.05$ meV (a Gaussian linewidth of 0.72 meV was used).
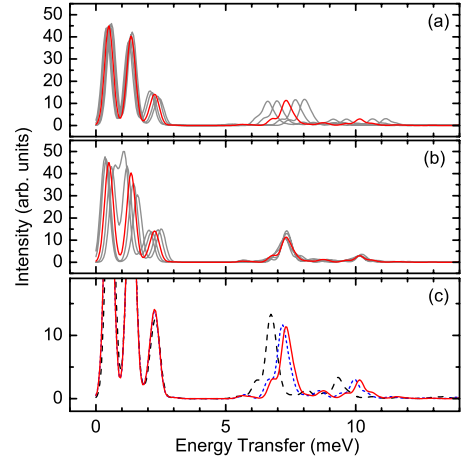

FIG. 7. (Color online) (a) Dependence of the INS spectrum on J, which is varied by a maximum of $\pm 10\%$ around a center value of $J = -1.79$ meV (red curve). The anisotropy is $D = -0.05$ meV. (b) Dependence of the INS spectrum on D, which is varied by a maximum $\pm 50\%$ around a center value of $D = -0.05$ meV (red curve). The coupling is $J = -1.79$ meV. (c) Dependence of the INS spectrum on a modulation of the J values along the ring. For all curves the anisotropy is $D = -0.05$ meV. Red (solid) curve: no modulation, $J_1 = J_2 = -1.79$ meV. Blue (short dashed) curve: $J_1 = -2.14$ meV and $J_2 = -1.45$ meV. Black (long dashed) curve: $J_1 = -2.48$ meV and $J_2 = -1.10$ meV.

$E_i = 25$ meV, $T = 5$ K. The two peaks III and IV are clearly visible, proving their magnetic origin.

The linewidths of the low-energy peaks Ia, Ib, and II lie within experimental accuracy determined by the instrumental resolution. In contrast, the linewidths of peaks III and IV are considerably broadened, as is most clearly seen in Fig. 5(b). However, our analysis will reveal that they consist of several close-lying transitions. Finally, it is interesting to note that in the energy regime above peak IV, i.e., above approximately 13 meV, no significant magnetic scattering intensity could be observed. In this regime, the scattering is entirely of phononic origin, as is evident from Fig. 6(a) and even more so from Fig. 5(a).

III. ANALYSIS

We have simulated the INS spectrum of Eq. (3) by calculating the energies and wave functions via a sparse-matrix exact numerical diagonalization method and using the formulas of Refs. 68 and 70. In order to find the parameters which yield the best fit to the experimental spectra we have systematically scanned the J and D parameter space, yielding $J = -1.79(5)$ meV and $D = -0.05(7)$ meV. These values are in excellent agreement with the previous findings.[66,67] The dependence of the simulated INS spectrum on J and D is shown in Figs. 7(a) and 7(b), respectively. The low-energy part of the spectrum is affected by both J and D. In contrast, the high-energy part is predominantly affected by J. Indeed, a 10% variation in J has a much larger effect than a 50% variation in D. This explains the rather large estimated standard deviation of the D value that we have determined. The
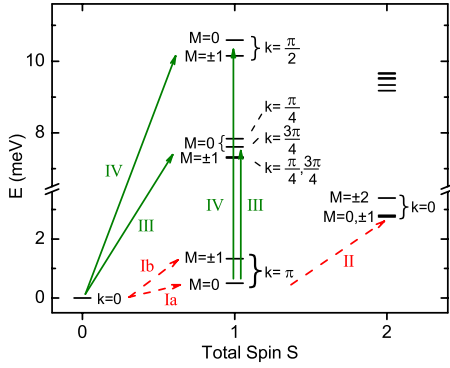
FIG. 8. (Color online) Calculated low-energy spectrum of Hamiltonian (3) with $J = -1.79$ meV and $D = -0.05$ meV. Only states in the sector $S \leq 2$ are plotted. The energy of the ground state was set to zero. Due to the anisotropy term, the degeneracy in M of each S multiplet is partially lifted. The relevant INS transitions are plotted as solid green (dashed red) arrows, marking transitions to the E band (L band).

simulated INS spectra corresponding to the best-fit values are shown at the bottom of Figs. 5(a) and 5(b) as solid lines, and as a $S(Q,\omega)$ plot in Fig. 6(b); the good agreement with the data is obvious.

Figure 8 shows the relevant part of the calculated spectrum, detailing the assignment of the observed peaks. The assignment of the lower-energy peaks has already been discussed in Refs. 66 and 67 and in the above. The peaks III and IV correspond to transitions from the $S = 0$ ground state to higher-lying $S = 1$ levels, which are slightly split due to the magnetic anisotropy. Accordingly, each of the peaks consists of a number of close-lying transitions, giving rise to the experimentally observed broadening of the peaks. Furthermore, at the measurement temperature of 5 K, also the transitions from the first excited state weakly contribute. The INS intensities of the individual transitions are indicated by the vertical thin lines in Fig. 5. The calculated contributions to all observed INS peaks, i.e., the quantum numbers of the involved states, the transition energies, and the scattering intensities, are detailed in Table I. The model Hamiltonian (3) assumes a perfect symmetry of the ring (i.e., an eightfold symmetry axis). However, though it is close to S_8, the molecular symmetry of $CsFe_8$ is C_4. Hence, weak deviations exist raising the question of how important they are for the magnetism in $CsFe_8$. This point is relevant for the understanding and explanation of phenomena such as the field-induced spin-Jahn-Teller effect[71–73] or the significance of possible Dzyaloshinski-Moriya (DM) interactions.[74] In this context, the present experiment is not sensitive to such small effects as a DM interaction or a biaxial anisotropy term (E term), but a variation in the exchange-coupling constants along the ring, e.g., in a J_1-J_2 alternating fashion, can be tested. Indeed, from general arguments it is expected that the L band states are rather insensitive to such a variation (as their energies are affected only in second order, see Ref. 65). However, this is not the case for the E band or spin-wave states, respectively, which hence provide a better means for a check. A simulation of the INS spectrum at 5 K with a modulation of the exchange-coupling constant of up to $\pm 40\%$

TABLE I. Calculated contributions to the observed INS transitions. The quantum states are labeled as $|S,M,k\rangle$, as in Fig. 8. The ground state is $|gs\rangle = |0,0,0\rangle$. $|i\rangle$ and $|f\rangle$ denotes the initial and final state in the transition. $E_f - E_i$ is the excitation energy in units of meV, and I_{if} indicates the transition strength, normalized to the strongest transition Ia. Transitions with strength $I_{if} < 0.05$ have been omitted.

Peak	$|i\rangle$	$|f\rangle$	$E_f - E_i$	I_{if}
Ia	$|gs\rangle$	$|1,0,\pi\rangle$	0.50	1.00
Ib	$|gs\rangle$	$|1,\pm 1,\pi\rangle$	1.34	0.97
II	$|1,\pm 1,\pi\rangle$	$|2,\pm 2,0\rangle$	2.05	0.06
	$|1,0,\pi\rangle$	$|2,0,0\rangle$	2.25	0.12
	$|1,0,\pi\rangle$	$|2,\pm 1,0\rangle$	2.30	0.20
III	$|1,0,\pi\rangle$	$|1,0,3\pi/4\rangle$	6.83	0.09
	$|gs\rangle$	$|1,\pm 1,3\pi/4\rangle$	7.30	0.33
	$|gs\rangle$	$|1,\pm 1,\pi/4\rangle$	7.33	0.05
	$|gs\rangle$	$|1,0,3\pi/4\rangle$	7.61	0.13
IV	$|gs\rangle$	$|1,0,\pi/2\rangle$	10.59	0.05
	$|gs\rangle$	$|1,\pm 1,\pi/2\rangle$	10.15	0.14

around its best-fit value is shown in Fig. 7(c). As expected, the low-energy part is not much affected but the spin-wave excitations at 7 and 10 meV have significantly moved toward lower energies. By comparison with the experimental widths of the peaks we conclude that a modulation of the exchange-coupling constants is smaller than $\pm 20\%$ in $CsFe_8$.

IV. DISCUSSION

In the previous sections the following points have been made: peaks III and IV are of magnetic origin, they are well reproduced by the generic spin Hamiltonian (3), they correspond to transitions from the ground state to excited $S = 1$ states, and there is negligible magnetic scattering at energies above peak IV. In this section we will discuss some implications of these findings.

As presented in Sec. I, the low-energy spectrum of AFM Heisenberg spin rings can be described by the RBM, which subdivides the spectrum into the L and E band; all other states are denoted collectively as the quasicontinuum. The L band is formed by the lowest-spin multiplet in each sector of total spin S. For $CsFe_8$, the transitions within the states of the L band were already investigated intensely before;[66,67] in the present work they are observed as peaks Ia, Ib, and II. The E band consists of the $N-2$ next higher-lying spin multiplets in each spin sector $S \geq 1$. These states are exactly those which are observed as the two peaks III and IV in our INS data. Only two broad INS peaks appear because of the (near) degeneracy of some states, which are due to the ring symmetry and the two-sublattice structure in the AFM ring, as will also become clear in the following. The RBM also predicts a selection rule for the matrix elements, which in fact is a key aspect of the RBM as it ultimately justifies the distinction of the states into the L band, E band, and quasicontinuum. It states that, starting from the ground state, only transitions to

states of the L or E band have significant INS intensities, while transitions into the quasicontinuum are negligibly weak. Thus, at low temperatures no magnetic INS intensity should be observed at energies above the E band or peak IV, respectively, exactly as observed in our experiment. Therefore, in conjunction with the previous work,[66,67] which confirmed the L band in great detail, the data presented here provides a thorough confirmation of the RBM for CsFe$_8$. This is only the second example where this has been achieved (the first being on the Cr$_8$ molecule, Ref. 30).

The connection between E band and quantized AFM spin waves has been discussed before in the literature to some extent.[45,46,49,50,60] In the following it will be made explicit by applying various SWTs available in the literature to a small AFM Heisenberg ring. The analysis will also give insight into the strengths and weaknesses of these methods when applied to small spin clusters. As it was shown in Sec. III, the energies of peaks III and IV do not depend much on the magnetic anisotropy. Hence, it is ignored in the calculations in this section, i.e., Eq. (1) is used. Excitation energies are given relative to the ground-state energy E_g.

It is useful to first discuss the symmetries of the model and Fig. 8. The AFM Heisenberg ring exhibits spin-rotational symmetry, which gives rise to quantum numbers S and M, and a D_N spatial symmetry. In a pure Heisenberg model the states are degenerate with respect to M. In CsFe$_8$ this degeneracy is lifted by the magnetic anisotropy, as indicated in Fig. 8, but the splitting is weak for the higher-lying states, and a classification in terms of spin multiplets or S, respectively, is useful. As regards the spatial symmetry, it is convenient to relax it to C_N. The quantum numbers, which we will call shift quantum number q, are related to a shift operator $\hat{T}|q\rangle = \exp(iq2\pi/N)|q\rangle$ with $q = 0, 1, \ldots, N-1$. Alternatively, one may use "wave vectors" $k = 2\pi q/N + \text{const}$, where we chose const such that for the ground state $k = 0$. The actual symmetry, however, is D_N, which requires that states with q and $N-q$, or k and $-k$, respectively, are degenerate. We now turn to Fig. 8. The $S = 0$ sector embraces the ground state with $k = 0$. The remaining $S = 0$ levels are high up in energy and are part of the quasicontinuum (not shown in Fig. 8). In the $S = 1$ sector, the (three) lowest states correspond to the first excited spin multiplet of the L band, for which $k = \pi$. This multiplet appears split in Fig. 8 because of the magnetic anisotropy. The next $N-2 = 6$ higher-lying spin multiplets with $k = \pm\frac{\pi}{4}, \pm\frac{\pi}{2}, \pm\frac{3\pi}{4}$ form the E band. Their counting is difficult in Fig. 8 because of the anisotropy splitting and the degeneracies. This pattern of states continues for $S > 1$ (not shown in Fig. 8).

Alternatively to the energy vs S representation, the structure of the energy spectrum may be discussed in an energy vs k representation, which for an infinite system would be the dispersion relation. However, in a small system, with no periodicity along an extended axis, k in general does not correspond to a "real" wave vector (although it can approach one for $N \to \infty$ in the case of a ring). Furthermore, k may assume only a set of finite values, and in consequence, the allowed energies are discrete values, yielding quantized spin waves in our context. All available SWTs can easily be applied to small spin clusters if one chooses to work in real
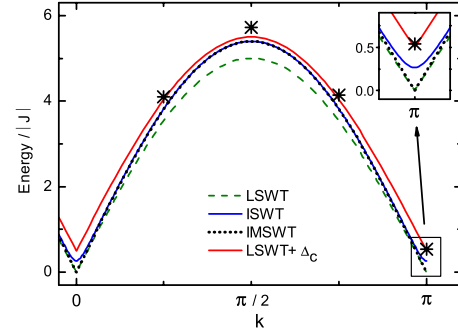

FIG. 9. (Color online) Spin-wave excitation energies as calculated by exact numerical diagonalization (stars) normalized to $|J|$ and the different SWTs (solid, dashed, and dotted lines) as discussed in the text. The abbreviations are LSWT: linear SWT, ISWT: interacting SWT, IMSWT: full-diagonalization interacting modified SWT, LSWT+Δ_c: linear SWT plus classical gap Δ_c.

space and not momentum space (see Refs. 59 and 75). Generally, SWTs work with bosonic excitations from the ground state, the magnons, or spin waves. The one-magnon excitations correspond to the L- and E-band states in the $S = 1$ sector. Other states may, in principle, be generated by multiple-magnon excitations but because of the technical difficulties SWT is rarely developed to this stage. In other words, the SWTs provide us with the energies of the L- and E-band states in the $S = 1$ sector or the values $\epsilon(k)$ in Eq. (2), respectively. The dependence on S is essentially out of their reach. The excitation energies of these states are plotted as a function of k in Fig. 9 for different SWTs as well as the exact numerical result.

In the early 1950s, the (conventional) linear and interacting SWTs were established.[13,15] Low-dimensional systems present a challenge since divergencies appear in 1D (and 0D) due to the fact that in these SWTs the modes with $k = 0$ and π are degenerate and have zero energy (Goldstone modes). The L band is related to these modes; hence the gap between the $S = 0$ ground state and the first excited $S = 1$ state (singlet-triplet gap), which in small AFM systems is always present, is zero, i.e., can never be reproduced by these SWTs. Later on, the modified SWTs (Refs. 17–19) and Schwinger-boson mean-field theory (SBMFT) (Refs. 76 and 77) were introduced, which eliminate the drawback of a zero singlet-triplet gap, suggesting their applicability to small spin clusters. Fortunately, for all these theories, linear SWT (LSWT), interacting SWT (ISWT), linear modified SWT (LMSWT), interacting modified SWT (IMSWT), and SBMFT, analytical results are available for 1D, which can be directly applied to the AFM ring (various IMSWTs exist, we have used the full-diagonalization IMSWT of Ref. 78). Interestingly, the SBMFT yields exactly the same excitation energies as the LMSWT, and also the ground-state energy agree after introduction of a correction factor.[78,79] Hence, there is no need to consider the SBMFT separately in the following. The singlet-triplet gap may be approximated by $\Delta_c = 4|J|/N$, which becomes exact in the classical limit.[13,49,50] Adding this gap to the excitation energies of the conventional SWTs is tempting (and may be justified, see Refs. 21 and 23) but does not improve the ISWT; the result for LSWT, denoted as LSWT+Δ_c, is discussed below.

TABLE II. Exact and SWT results for the singlet-triplet gap, energy width, and mean deviation for a $N=8$, $s=5/2$ ring.

	$E_g/\lvert J\rvert$	$\Delta/\lvert J\rvert$	$[\epsilon(k=\pi/2)-\Delta]/\lvert J\rvert$	χ^2
Exact	−58.1105	0.537	5.180	0
LSWT	−57.2600	0	5	0.133
LMSWT	−57.8049	0.248	4.758	0.115
ISWT	−58.2433	0	5.396	0.093
IMSWT	−58.1095	0.268	5.129	0.065
LSWT+Δ_c		0.5	5	0.025

The excitation energies as function of k are presented in Fig. 9. The interpretation of the INS transitions in terms of spin waves is obvious: peak IV at 10 meV corresponds to the one-magnon excitations with $k=\pm\frac{\pi}{2}$, and peak III at 7 meV is related to excitations of magnons with $k=\pm\frac{\pi}{4}$ and $\pm\frac{3\pi}{4}$. The "quantization" of the spin-wave energies due to the system's finite size can also be regarded as being due to a "confinement" of the magnons in three-dimensional space. The dispersion relation as calculated by SWT is also symmetric with respect to $k=\pm\frac{\pi}{4}$ due to the AFM sublattice structure.

Table II compiles the ground-state energy E_g, singlet-triplet gap Δ,[80] width $\epsilon(\pi/2)-\epsilon(\pi)$ of the excitation spectrum, and mean deviation $\chi^2=\Sigma_k[\epsilon(k)-\epsilon_{\text{exact}}(k)]^2/(\frac{1}{2}N\lvert J\rvert s)$ from the exact energies as calculated by exact numerical diagonalization and the various SWTs for the case $N=8$, $s=5/2$. Inspection of Table II and Fig. 9 shows: (1) as discussed beforehand the conventional SWTs (LSWT and ISWT) do not produce a singlet-triplet gap while the modified SWTs do. Yet, they grossly underestimate the gap, by a factor of 2. In contrast, the classical estimate Δ_c is off by only 7%. Hence, although the modified SWTs reproduce the singlet-triplet gap, they do not provide a good description of the low-energy or low-temperature behavior, respectively. Accordingly, LSWT+Δ_c performs best. (2) The width $\epsilon(\pi/2)-\epsilon(\pi)$ of the spin-wave excitation spectrum is obtained reasonably well in all considered SWTs with the expected trend that the interacting versions do better. Except for the ISWT, the SWTs underestimate the width. It is noted that the modified SWTs generally predict a smaller width than the corresponding conventional SWTs. Further, among the SWTs, IMSWT yields the best assessment of the excitations. Notably, the empirical LSWT+Δ_c calculation performs even better than the IMSWT. (3) Regarding the ground-state energy, the IMSWT yields the best results with a remarkably small deviation of only 0.002%. This implies that also the ground-state wave function is accurately obtained by this method. It would be interesting to verify this in the future.

V. CONCLUSION

In conclusion, we have observed by INS the excitation of quantized spin-wave modes in the molecule CsFe$_8$, i.e., an eight-membered AFM Heisenberg ring. Only a small number of discrete points on the $\epsilon(k)$ spin-wave dispersion curve are allowed due to the confinement of the magnetic excitations to the ring. Further, the INS data revealed that at low temperatures the magnetic scattering intensity at energies above the most energetic spin-wave excitation is negligibly small. These findings, combined with the demonstration of the L band in previous works, establish a thorough confirmation of the RBM for CsFe$_8$. We have compared several SWTs with numerically exact results. The full-diagonalization interacting modified SWT delivers excellent approximations to the ground-state energy and spin-wave excitations but the singlet-triplet gap and hence the low-temperature properties of the ring are only qualitatively reproduced. Regarding the excitation energies the empirical LSWT+Δ_c calculation performs best.

---

*jan.dreiser@physik.uni-freiburg.de

†oliver.waldmann@physik.uni-freiburg.de

‡Present address: Spallation Neutron Source, Oak Ridge National Laboratory, Oak Ridge, Tennessee 37831, USA.

[1] A. R. Rocha, V. M. García-suárez, S. W. Bailey, C. J. Lambert, J. Ferrer, and S. Sanvito, Nature Mater. **4**, 335 (2005).

[2] L. Bogani and W. Wernsdorfer, Nature Mater. **7**, 179 (2008).

[3] C. Schlegel, J. van Slageren, M. Manoli, E. K. Brechin, and M. Dressel, Phys. Rev. Lett. **101**, 147203 (2008).

[4] S. Bertaina, S. Gambarelli, T. Mitra, B. Tsukerblat, A. Müller, and B. Barbara, Nature (London) **453**, 203 (2008).

[5] M. Mannini, F. Pineider, P. Sainctavit, C. Danieli, E. Otero, C. Sciancalepore, A. M. Talarico, M.-A. Arrio, A. Cornia, D. Gatteschi, and R. Sessoli, Nature Mater. **8**, 194 (2009).

[6] J. des Cloizeaux and J. J. Pearson, Phys. Rev. **128**, 2131 (1962).

[7] Zheng Weihong and C. J. Hamer, Phys. Rev. B **47**, 7961 (1993).

[8] P. V. Hendriksen, S. Linderoth, and P.-A. Lindgård, Phys. Rev. B **48**, 7259 (1993).

[9] C. Mathieu, J. Jorzick, A. Frank, S. O. Demokritov, A. N. Slavin, B. Hillebrands, B. Bartenlian, C. Chappert, D. Decanini, F. Rousseaux, and E. Cambril, Phys. Rev. Lett. **81**, 3968 (1998).

[10] J. Jorzick, S. O. Demokritov, B. Hillebrands, M. Bailleul, C. Fermon, K. Y. Guslienko, A. N. Slavin, D. V. Berkov, and N. L. Gorn, Phys. Rev. Lett. **88**, 047204 (2002).

[11] J. Podbielski, F. Giesen, and D. Grundler, Phys. Rev. Lett. **96**, 167207 (2006).

[12] J. Topp, J. Podbielski, D. Heitmann, and D. Grundler, Phys. Rev. B **78**, 024431 (2008).

[13] P. W. Anderson, Phys. Rev. **86**, 694 (1952).

[14] R. Kubo, Phys. Rev. **87**, 568 (1952).

[15] T. Oguchi, Phys. Rev. **117**, 117 (1960).

[16] M. Takahashi, Phys. Rev. Lett. **58**, 168 (1987).

[17] M. Takahashi, Phys. Rev. B **40**, 2494 (1989).

[18] J. E. Hirsch and S. Tang, Phys. Rev. B **40**, 4769 (1989).

[19] S. Tang, M. E. Lazzouni, and J. E. Hirsch, Phys. Rev. B **40**, 5000 (1989).

[20] S. M. Rezende, Phys. Rev. B **42**, 2589 (1990).

[21] Q. F. Zhong and S. Sorella, Europhys. Lett. **21**, 629 (1993).

[22] C. Lavalle, S. Sorella, and A. Parola, Phys. Rev. Lett. **80**, 1746 (1998).

[23] A. E. Trumper, L. Capriotti, and S. Sorella, Phys. Rev. B **61**, 11529 (2000).

[24] S. Itoh, Y. Endoh, K. Kakurai, and H. Tanaka, Phys. Rev. Lett. **74**, 2375 (1995).

[25] N. B. Ivanov and P. Ch. Ivanov, Phys. Rev. B **46**, 8206 (1992).

[26] R. Wieser, E. Y. Vedmedenko, and R. Wiesendanger, Phys. Rev. Lett. **101**, 177202 (2008).

[27] S. T. Ochsenbein, O. Waldmann, A. Sieber, G. Carver, R. Bircher, H. U. Güdel, R. S. G. Davies, G. A. Timco, R. E. P. Winpenny, H. Mutka, and F. Fernandez-Alonso, Europhys. Lett. **79**, 17003 (2007).

[28] S. T. Ochsenbein, F. Tuna, M. Rancan, R. S. G. Davies, C. A. Muryn, O. Waldmann, R. Bircher, A. Sieber, G. Carver, H. Mutka, F. Fernandez-Alonso, A. Podlesnyak, L. P. Engelhardt, G. A. Timco, H. U. Güdel, and R. E. P. Winpenny, Chem.-Eur. J. **14**, 5144 (2008).

[29] G. Chaboussant, A. Sieber, S. Ochsenbein, H.-U. Güdel, M. Murrie, A. Honecker, N. Fukushima, and B. Normand, Phys. Rev. B **70**, 104422 (2004).

[30] O. Waldmann, T. Guidi, S. Carretta, C. Mondelli, and A. L. Dearden, Phys. Rev. Lett. **91**, 237202 (2003).

[31] S. Yamamoto and T. Nakanishi, Phys. Rev. Lett. **89**, 157603 (2002).

[32] H. Hori and S. Yamamoto, Phys. Rev. B **68**, 054409 (2003).

[33] D. Gatteschi and R. Sessoli, *Molecular Nanomagnets* (Oxford University Press, New York, 2006).

[34] B. Barbara, L. Thomas, F. Lionti, I. Chiorescu, and A. Sulpice, J. Magn. Magn. Mater. **200**, 167 (1999).

[35] G. Christou, D. Gatteschi, D. N. Hendrickson, and R. Sessoli, MRS Bull. **25** (11), 66 (2000).

[36] D. Gatteschi and R. Sessoli, Angew. Chem., Int. Ed. **42**, 268 (2003).

[37] W. Wernsdorfer, Adv. Chem. Phys. **118**, 99 (2007).

[38] K. L. Taft, C. D. Delfs, G. C. Papaefthymiou, S. Foner, D. Gatteschi, and S. J. Lippard, J. Am. Chem. Soc. **116**, 823 (1994).

[39] M.-H. Julien, Z. H. Jang, A. Lascialfari, F. Borsa, M. Horvatic, A. Caneschi, and D. Gatteschi, Phys. Rev. Lett. **83**, 227 (1999).

[40] A. Cornia, A. G. M. Jansen, and M. Affronte, Phys. Rev. B **60**, 12177 (1999).

[41] J. van Slageren, R. Sessoli, D. Gatteschi, A. A. Smith, M. Helliwell, R. E. P. Winpenny, A. Cornia, A.-L. Barra, A. G. M. Jansen, E. Rentschler, and G. A. Timco, Chem.-Eur. J. **8**, 277 (2001).

[42] S. Carretta, J. van Slageren, T. Guidi, E. Liviotti, C. Mondelli, D. Rovai, A. Cornia, A. L. Dearden, F. Carsughi, M. Affronte, C. D. Frost, R. E. P. Winpenny, D. Gatteschi, G. Amoretti, and R. Caciuffo, Phys. Rev. B **67**, 094405 (2003).

[43] B. Pilawa, R. Boffinger, I. Keilhauer, R. Leppin, I. Odenwald, W. Wendl, C. Berthier, and M. Horvatic, Phys. Rev. B **71**, 184419 (2005).

[44] P. W. Anderson, *Basic Notions of Condensed Matter Physics* (Benjamin/Cummings, Menlo Park, 1984).

[45] B. Bernu, C. Lhuillier, and L. Pierre, Phys. Rev. Lett. **69**, 2590 (1992).

[46] B. Bernu, P. Lecheminant, C. Lhuillier, and L. Pierre, Phys. Rev. B **50**, 10048 (1994).

[47] A. Chiolero and D. Loss, Phys. Rev. Lett. **80**, 169 (1998).

[48] J. Schnack and M. Luban, Phys. Rev. B **63**, 014418 (2000).

[49] O. Waldmann, Phys. Rev. B **65**, 024424 (2001).

[50] C. Lhuillier, arXiv:cond-mat/0502464 (unpublished).

[51] T. Guidi, S. Carretta, P. Santini, E. Liviotti, N. Magnani, C. Mondelli, O. Waldmann, L. K. Thompson, L. Zhao, C. D. Frost, G. Amoretti, and R. Caciuffo, Phys. Rev. B **69**, 104432 (2004).

[52] R. Caciuffo, T. Guidi, G. Amoretti, S. Carretta, E. Liviotti, P. Santini, C. Mondelli, G. Timco, C. A. Muryn, and R. E. P. Winpenny, Phys. Rev. B **71**, 174407 (2005).

[53] O. Waldmann, Coord. Chem. Rev. **249**, 2550 (2005).

[54] P. Santini, S. Carretta, G. Amoretti, T. Guidi, R. Caciuffo, A. Caneschi, D. Rovai, Y. Qiu, and J. R. D. Copley, Phys. Rev. B **71**, 184405 (2005).

[55] O. Waldmann, H. U. Güdel, T. L. Kelly, and L. K. Thompson, Inorg. Chem. **45**, 3295 (2006).

[56] T. Guidi, J. R. D. Copley, Y. Qiu, S. Carretta, P. Santini, G. Amoretti, G. Timco, R. E. P. Winpenny, C. L. Dennis, and R. Caciuffo, Phys. Rev. B **75**, 014408 (2007).

[57] J. Schnack, M. Luban, and R. Modler, Europhys. Lett. **56**, 863 (2001).

[58] V. O. Garlea, S. E. Nagler, J. L. Zarestky, C. Stassis, D. Vaknin, P. Kögerler, D. F. McMorrow, C. Niedermayer, D. A. Tennant, B. Lake, Y. Qiu, M. Exler, J. Schnack, and M. Luban, Phys. Rev. B **73**, 024414 (2006).

[59] O. Waldmann, Phys. Rev. B **75**, 012415 (2007).

[60] G. Müller, H. Thomas, H. Beck, and J. C. Bonner, Phys. Rev. B **24**, 1429 (1981).

[61] F. D. M. Haldane, Phys. Rev. Lett. **50**, 1153 (1983).

[62] J. Schnack, Phys. Rev. B **62**, 14855 (2000).

[63] L. Engelhardt and M. Luban, Phys. Rev. B **73**, 054430 (2006).

[64] R. W. Saalfrank, I. Bernt, E. Uller, and F. Hampel, Angew. Chem., Int. Ed. Engl. **36**, 2482 (1997).

[65] O. Waldmann, R. Koch, S. Schromm, J. Schülein, P. Müller, I. Bernt, R. W. Saalfrank, F. Hampel, and E. Balthes, Inorg. Chem. **40**, 2986 (2001).

[66] O. Waldmann, C. Dobe, H. U. Güdel, and H. Mutka, Phys. Rev. B **74**, 054429 (2006).

[67] O. Waldmann, C. Dobe, H. Mutka, A. Furrer, and H. U. Güdel, Phys. Rev. Lett. **95**, 057202 (2005).

[68] O. Waldmann, Phys. Rev. B **68**, 174406 (2003).

[69] G. Shirane, S. M. Shapiro, and J. M. Tranquada, *Neutron Scattering with a Triple-Axis Spectrometer* (Cambridge University Press, Cambridge, England, 2002).

[70] O. Waldmann and H. U. Güdel, Phys. Rev. B **72**, 094422 (2005).

[71] O. Waldmann, C. Dobe, S. T. Ochsenbein, H. U. Güdel, and I. Sheikin, Phys. Rev. Lett. **96**, 027206 (2006).

[72] A. Soncini and L. F. Chibotaru, Phys. Rev. Lett. **99**, 077204 (2007).

[73] V. Lante, I. Rousochatzakis, K. Penc, O. Waldmann, and F. Mila, Phys. Rev. B **79**, 180412(R) (2009).

[74] F. Cinti, M. Affronte, and A. Jansen, Eur. Phys. J. B **30**, 461 (2002).

[75] O. Cépas and T. Ziman, Prog. Theor. Phys. Suppl. **159**, 280 (2005).

[76] A. Auerbach and D. P. Arovas, Phys. Rev. Lett. **61**, 617 (1988).

[77] S. Sarker, C. Jayaprakash, H. R. Krishnamurthy, and M. Ma, Phys. Rev. B **40**, 5028 (1989).

[78] S. Yamamoto and H. Hori, J. Phys. Soc. Jpn. **72**, 769 (2003).

[79] D. P. Arovas and A. Auerbach, Phys. Rev. B **38**, 316 (1988).

[80] We define the singlet-triplet gap in the case of SWTs as $\Delta = \epsilon(\pi)$.